



Three-Dimensional Structure Analysis and Percolation Properties of a Barrier Marine Coating

Bo Chen^{1,7}, Manuel Guizar-Sicairos², Gang Xiong¹, Laura Shemilt¹, Ana Diaz², John Nutter¹, Nicolas Burdet¹, Suguo Huo¹, Joel Mancuso³, Alexander Monteith⁴, Frank Vergeer⁵, Andrew Burgess⁶ & Ian Robinson^{1,7}

¹London Centre for Nanotechnology, University College London, WC1H 0AH, UK, ²Paul Scherrer Institut, 5232 Villigen PSI, Switzerland, ³Gatan, Inc., Pleasanton, California 94588, USA, ⁴Gatan (UK) Ltd., Abingdon, Oxfordshire, OX14 1RL, UK, ⁵AkzoNobel Co. Ltd., Sassenheim, 2171AJ, the Netherlands, ⁶AkzoNobel (UK) Co. Ltd., Felling, Gateshead, Tyne and Wear, NE10 0JY, UK, ⁷Research Complex at Harwell, Harwell Oxford, Didcot, Oxfordshire, OX11 0FA, UK.

Received
15 October 2012

Accepted
9 January 2013

Published
31 January 2013

Correspondence and requests for materials should be addressed to B.C. (chenwillcon@gmail.com) or I.R. (i.robinson@ucl.ac.uk)

Artificially structured coatings are widely employed to minimize materials deterioration and corrosion, the annual direct cost of which is over 3% of the gross domestic product (GDP) for industrial countries. Manufacturing higher performance anticorrosive coatings is one of the most efficient approaches to reduce this loss. However, three-dimensional (3D) structure of coatings, which determines their performance, has not been investigated in detail. Here we present a quantitative nano-scale analysis of the 3D spatial structure of an anticorrosive aluminium epoxy barrier marine coating obtained by serial block-face scanning electron microscopy (SBFSEM) and ptychographic X-ray computed tomography (PXCT). We then use finite element simulations to demonstrate how percolation through this actual 3D structure impedes ion diffusion in the composite materials. We found the aluminium flakes align within 15° of the coating surface in the material, causing the perpendicular diffusion resistance of the coating to be substantially higher than the pure epoxy.

Barrier coatings, an essential branch of the corrosion-resistant coating family, are deliberately structured to operate in extremely aggressive environments such as seawater^{1–3} to prevent corrosion of substrate materials^{4,5}. Among these coatings, the aluminium flake pigmented epoxy coatings are widely applied to protect steel structures such as ocean-going vessels because of their excellent anticorrosive performance¹, as determined by their diffusion barrier properties². The shape and spatial distribution of the aluminium flakes, usually several microns wide and a few hundred nanometres thick, added to the materials significantly improve the barrier properties by decreasing the transport rate of corrosive substances such as ions, water (vapour) and oxygen through coating films^{1,2,6}. Additionally, the aluminium can react with the hydroxide ions produced at the cathode in the corrosion cell, reducing the pH at the coating-steel interface and decreasing the rate of cathodic disbondment⁷. Meanwhile, the epoxy resin gives the coating film abrasion resistance and functions as a corrosion inhibitor for the aluminium flakes⁸. However, the 3D structure of the coatings^{9,10} has not been accessed in detail before.

Here we studied an anticorrosive aluminium epoxy barrier marine coating composed of aluminium flakes, talc fragments, iron oxide particles and epoxy resin (matrix material). The measured coating samples were prepared by, firstly, introducing the pigment ingredients including aluminium flakes, talc fragments and iron oxide particles into the epoxy resin using high shear mixing until the pigment particles are appropriately dispersed. The amine curing agent was then added into the pigmented epoxy resin at 1 : 1 stoichiometry. The epoxy resin and amine curing agent were mixed immediately prior to coating application. The coating material was then applied on the substrate and used to prepare two types of samples. The non-degassed coating was obtained by directly curing the applied material at 100°C for an hour and then curing at room temperature for one month. The degassed coating was treated by an extra degassing procedure in vacuum before experienced the same curing process as the non-degassed coating. The former procedure is the traditional method; the latter degassing procedure could lead to potential improvements of coating technology.

Both aluminium flakes and talc fragments work as barriers when they align parallel to the coating surface. In commercial products, talc fragments substitute for aluminium flakes to reduce cost as well as the risk of electrical



sparking. The iron oxide particles are added to produce the desired colour and to improve solvent and chemical resistance of the products¹¹. Serial block-face scanning electron microscopy (SBFSEM)¹² and ptychographic X-ray computed tomography (PXCT)^{13,14} were employed for the purpose, after we found that full-field transmission X-ray microscopy using both laboratory and synchrotron sources could not reveal the contrast between the various internal structures of the material.

Results

SBFSEM, a serial sectioning imaging method^{12,15,16}, was used to image a degassed sample. The technique was originally developed for 3D spatial structure investigation of biological specimens^{17–19}, from ultrathin section sample preparation for transmission electron microscopy (TEM)²⁰. It acquires a continuous series of parallel images of fresh surfaces created by mechanical cuts made by a diamond knife installed in an ultramicrotome¹². Three-dimensional (3D) images of samples are then generated by stacking the corresponding series of images together.

A degassed and a non-degassed sample of the same material were imaged by PXCT which combines scanning coherent X-ray diffractive imaging^{21,22} with computed tomography^{23,24}. Both samples were first cut to size using a focused ion beam (FIB) tool. A tomographic projection at each rotation angle was reconstructed from multiple X-ray diffraction patterns using a difference-map phase-retrieval algorithm²². PXCT produces quantitative 3D images of customised field of view with a representation of the average electron density per voxel^{13,25}. It avoids mechanical sample destruction and possible cutting artefacts which, in certain cases, can be detrimental to nano- and micro-scale sciences.

Figure 1a is a contrast-reversed back scattering electron (BSE) image of the degassed aluminium epoxy barrier marine coating from

the SBFSEM measurement. Flake-shaped dark objects, grey objects and small black dots in it were identified as aluminium flakes, talc fragments and iron oxide particles, respectively, as segmented by commercial software “Avizo” and shown in figure 1b as dark-grey objects, light-grey objects and bright small spots. The remaining parts of figures 1a and 1b were attributed to epoxy resin. This segmentation was validated by the quantitative values of electron density obtained with PXCT, as discussed below. The 3D spatial arrangement of aluminium flakes within the material is illustrated in figure 1e (and as the supplementary movie 1), in which we can see a parallel arrangement of the aluminium flakes that cannot be observed in 2D slice images.

Figure 2a presents a single reconstructed tomogram slice of a different piece of the same degassed sample obtained by the PXCT measurement. Here, the electron density is determined accurately enough for the components to be easily identified by the respective peaks of the density histogram, shown in figure 2b. The long, slim grey objects with electron density $0.793 \times 10^{30}/\text{m}^3$ are identified as aluminium flakes, the slightly brighter grey objects with electron density $0.905 \times 10^{30}/\text{m}^3$ are talc fragments, the small dots are iron oxide particles, the other grey parts are epoxy resin and the black regions are surrounding air. Upon conversion²⁵, the aluminium and talc mass densities are measured to be $2.73 \times 10^3 \text{ kg}/\text{m}^3$ and $3.00 \times 10^3 \text{ kg}/\text{m}^3$, compared with $2.70 \times 10^3 \text{ kg}/\text{m}^3$ and $2.78 \times 10^3 \text{ kg}/\text{m}^3$ from standard tables. The high contrast and boundary well-defined features generated in the tomogram slices enable their direct 3D segmentation into spatial volume regions. Figures 2d and 2e are 3D renderings (and as the supplementary movie 2) after segmentation, analogous to figures 1d and 1e, again presenting the parallel alignment of the aluminium flakes distinctly. PXCT demonstrates here its combined advantages of ptychography²¹, a phase-sensitive imaging technique, and X-ray computed tomography.

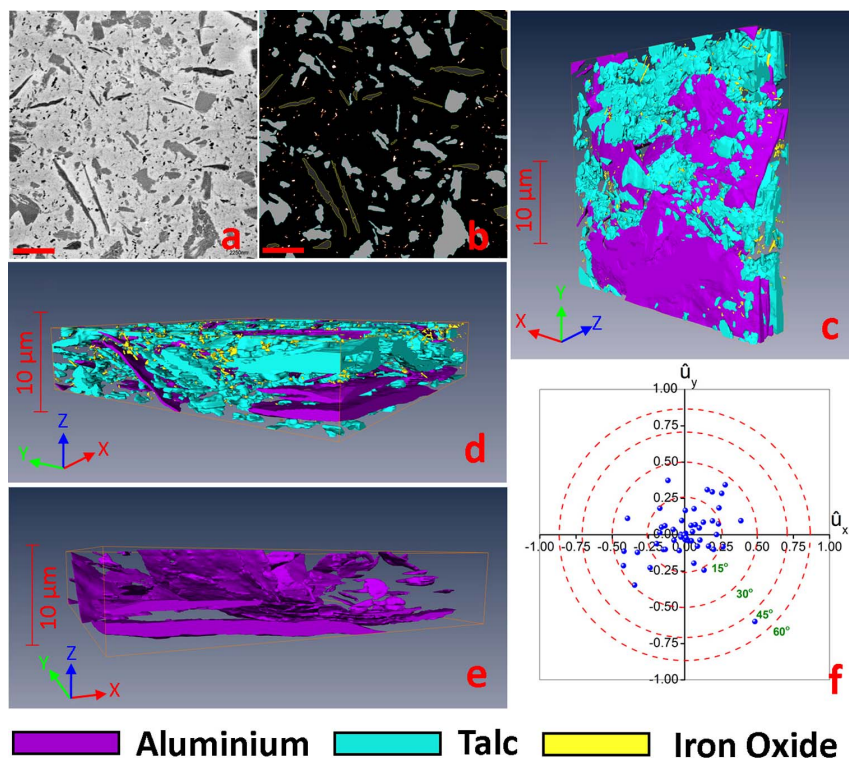


Figure 1 | Results for the degassed aluminium epoxy marine coating imaged by SBFSEM. (a) An SBFSEM single slice. (b) Segmented result from figure 1a. (c & d) Rendering of 3D spatial structure image of the coating. (e) A 3D image of just the aluminium flakes in the coating. (f) Quantitative orientation analysis of the aluminium flakes in the coating material. Deviation projections of individual flakes are plotted stereographically around the surface direction (centre). Dash circles denote net 15°, 30°, 45° and 60° deviations from parallel alignment to the surface. The scale bars in a and b are 5 microns.

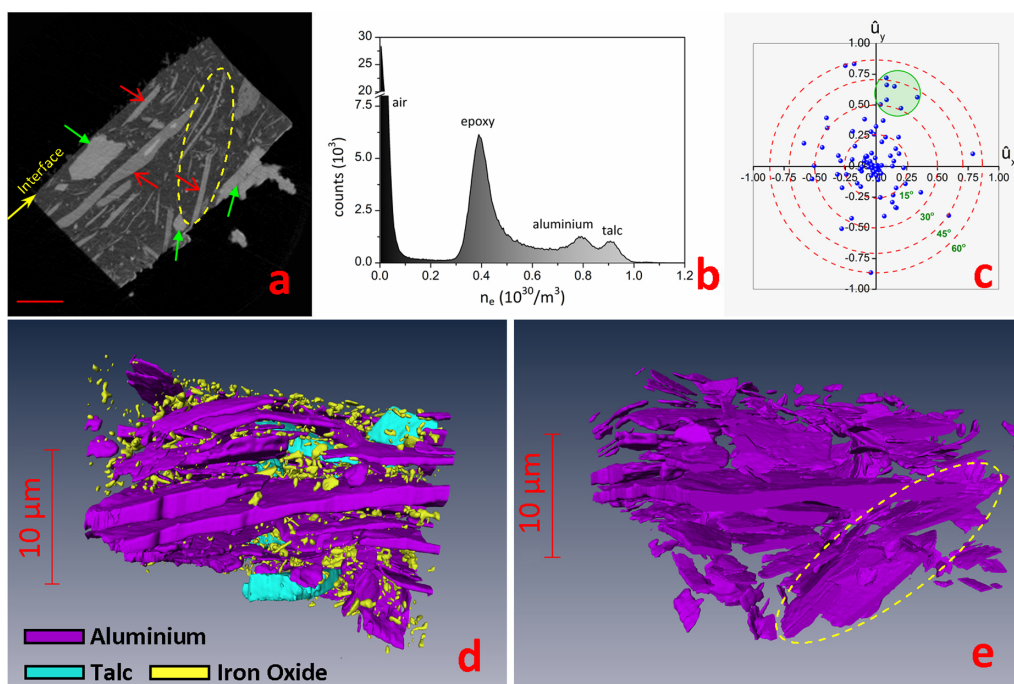


Figure 2 | Results for the degassed coating imaged by PXCT. (a) A single tomogram slice perpendicular to the rotation axis. Arrows point to some of the identified aluminium flakes in red and talc fragments in green. The scale bar is 5 microns. (b) Histogram of electron density distribution of the tomogram slice in figure 2a. (c) Quantitative orientation analysis of the aluminium flakes, plotted in the same way as figure 1f. (d) Rendering of 3D spatial structure image of the sample. (e) 3D spatial arrangement image of just the aluminium flakes in the material.

According to the sample mounting geometry (see Methods), the xy plane in figures 1c, d and e is parallel to the sample surface. The coating-steel interface in figure 2a is labelled and is assumed to be parallel to the sample surface. The surface normal direction of each aluminium flake is defined as the orientation of its major principal inertia axis which is along the shortest geometrical axis of the object. We find that the aluminium flakes arrange nearly parallel to the coating sample surfaces, mostly within 15° deviation, as shown in the orientation stereograms in figures 1f and 2c (see details in supplementary methods). A group of misoriented flakes, having around 40° deviation, is highlighted by a green circle in figure 2c. These flakes form a physical cluster lying next to each other in the material, as can be observed in the top-right of figure 2a or the lower-right part of figure 2e (circled by dashed yellow ellipses).

In addition, the lengths and volumes of individual objects in the materials can be obtained from morphometric analysis after the 3D image segmentation. Thus, the size of each object and the pigment volume concentration (PVC), one of the most crucial formulating parameters of coating products, of the applied and in-service coatings can be revealed. These parameters of the aluminium flakes are tabulated in the supplementary materials.

An interesting discovery in the non-degassed aluminium epoxy marine coating is that the aluminium flakes tend to follow the edges of nearby air pores, as seen in figure 3. This correlation in structure has not been observed before, and it is different from the common expectation that the aluminium flakes should be parallel to the external coating surface. This may be due to a surface alignment effect at the edges of air pores which is similar to that at the external coating surface, which is caused by solvent evaporation during the drying process¹¹. The volume exclusion effect may arise simply because when, the air bubbles in the coating material nucleate and grow, they push the aluminium flakes to their periphery. This co-localised structure may be responsible for the strong barrier function against corrosive substances in the pores, which are presumably the penetration point for external agents and which provide space for accumulation of corrosive substances. However, this structure has

the potential hazard that, once the aluminium flakes become eroded, the anticorrosive performance/protective capability of the coating would suddenly diminish because of decomposition of the barriers.

Simulations of the percolation properties of the coating were performed using COMSOL “MultiPhysics” software package, based on the actual, segmented 3D spatial structures instead of modelling structures²⁶. We determined the ion diffusion process in the coating films, which is regarded as the rate-determining process governing the cathodic delamination of coatings from steel and its corrosion². The simulations were done by calculating electric conductivity σ in the materials following Ohm’s law ‘ $J = -\sigma \nabla V$ ’ which has the same mathematical form as Fick’s first law ‘ $J = -D \nabla C$ ’ that can describe diffusion in 3D systems when the concentration of the diffusing species can be assumed to remain constant. J is the current density or (ion) diffusion flux, ∇V is the potential gradient (locally the

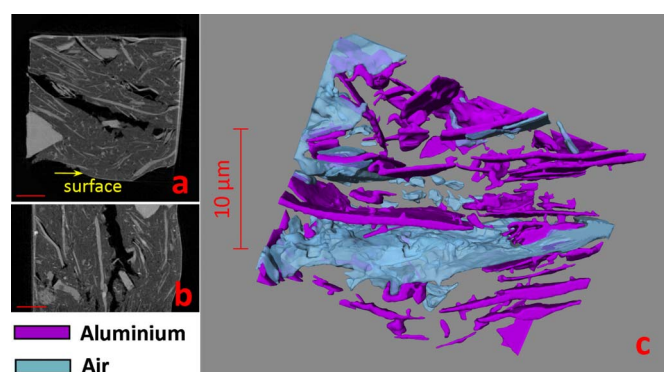


Figure 3 | Results for the non-degassed aluminium epoxy marine coating from PXCT measurement. (a & b) Tomogram slices perpendicular and parallel to the rotation axis through the reconstructed 3D volume, respectively. In figure 3b, the image plane is parallel to the coating surface. (c) Rendering of 3D spatial arrangement of aluminium flakes and air pores in the sample. The scale bars in a and b are 5 microns.

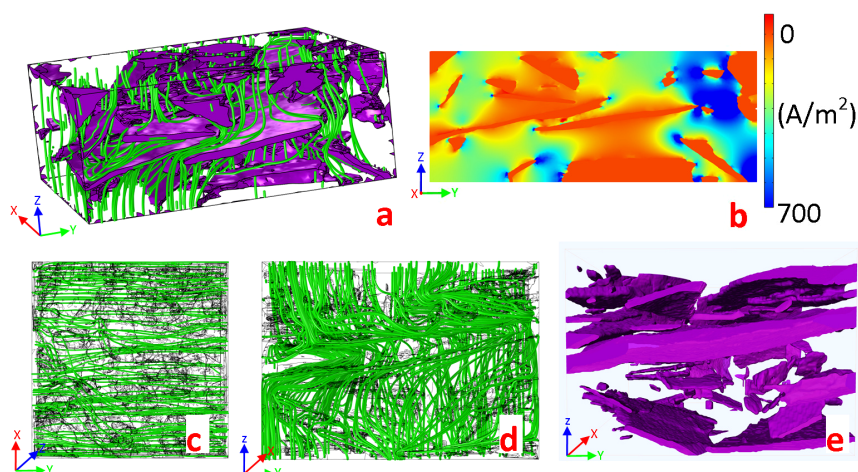


Figure 4 | Finite element simulation results based on the actual 3D spatial structures of the coating measured in this study. (a) Simulated flow along the direction perpendicular to the coating surface presented as streamlines within the real structure obtained from the SBFSEM measurement. (b) A slice cut of the current density map generated from simulation in panel a. (c & d) Simulated flow along the directions parallel and perpendicular to the coating surface of the structure obtained by PXCT. (e) Rendering of the 3D volume of the coating structure used for simulations in panels (c) and (d).

potential difference, V , divided by the conductor length), D is the diffusion coefficient and ∇C is the concentration gradient. The ion diffusion and electric conduction are also relevant because both ions and electrons are charged particles and the potential difference is a driving force for ion transport during the electrochemical process of steel corrosion. The electric conductivities were calculated along the directions perpendicular and parallel to the coating surface directions to determine the material's diffusion coefficient anisotropy $R = \sigma_{\text{perpendicular}}/\sigma_{\text{parallel}}$.

Figures 4a, c and d present the simulation results as streamlines of flow, which are the paths followed by ions from one side to the other of the coating films during diffusion. The ions flow along surfaces of objects and go around the obstructions in the structures, which clearly reveals the barrier properties of aluminium flakes against ions. This validates, with direct evidence, the pictorial matrix models of barrier coatings found in the literature²⁷. The current density map (figure 4b) illustrates the ions have much higher concentrations at the edges of flakes which could potentially become the points that corrosion starts. It may be worth applying extra protective treatment to the edges of the aluminium flakes.

The simulation based on the SBFSEM structure (figure 4a), 6 microns thick, shows the diffusion coefficient anisotropy to be $R = 0.516$. The 10 microns thick structure obtained from PXCT (figure 4e) gave $R = 0.358$. The smaller anisotropy ratio acquired in the latter case could be caused by a single big aluminium flake in the structure (see figure 4e) which occupies the majority area of the cross-section and blocks the transport routes of ions more drastically. Therefore, trying to avoid breaking aluminium flakes either during manufacture or application process would contribute to improving the final performance of the coating films. Considering the not-quite parallel alignment of the aluminium flakes to the coating surface, we could expect that pure epoxy would give higher ion diffusion coefficient and smaller anisotropy ratio value against the surface perpendicular direction. This illustrates that the diffusion rate of ions across the aluminium flakes pigmented coating is heavily reduced compared with pure epoxy.

Discussion

The morphological analysis of 3D spatial structures and the simulations performed on them reveal the relations between the structure of coatings and their properties. The results from SBFSEM and PXCT validated each other and both methods were proved to be effective ways to measure 3D spatial structures of complex industrial

specimens. Compared with PXCT, SBFSEM provides higher resolution and avoids employing iterative phase-retrieval algorithms. However, it is a destructive method because the diamond knife has direct physical contact with the imaging surfaces, which could potentially lead to deformation of shapes and movement of positions of features in the samples. PXCT is found to be especially powerful at quantitative (structural) characterisation as it shows the ability to distinguish the four components in the material quantitatively by electron density. In principle, it is a non-destructive method which should preserve the sample structure well during measurement. By taking measured 3D structures into detailed simulations, we have demonstrated an approach for validating mechanistic assumptions and potentially provide a practical method to engineer the efficacy of anti-corrosion coatings by modelling electrochemical process in materials based on the actual structures. This could be used to evaluate the performance of materials, and shorten the product research and development lifetime, compared with carrying out endurance studies of original specimens, which can take years. We found that the degassed specimens have more compact structure comparing with the non-degassed one prepared by conventional coating technology, which means the former would provide better anti-corrosive properties. The degassing treatment could be used to enhance coating performance and thus to further reduce the risk of steel construction failures such as oil tanker break-ups.

Methods

SBFSEM measurement. The degassed aluminium epoxy barrier marine coating film was mounted on an aluminium specimen pin (Gatan, Inc.) using cyanoacrylate glue. The coating surface was placed perpendicular to the axis of the pin. The sample was then trimmed down by a microtome to create a block face sizes approximately $500 \mu\text{m} \times 500 \mu\text{m}$. After that, it was measured by the SBFSEM system, installed in an environmental SEM and operated at 2.5 kV with 0.4 Torr chamber pressure in a water vapour environment. The BSE signals from the sample were acquired with 10 μs dwell time per pixel of size $30 \text{ nm} \times 30 \text{ nm}$, at a working distance of 5.8 mm. The sectioning thickness was 30 nm per slice with a cutting speed 22 s per slice. Altogether 200 slice images (6 μm thick) with a field of view $30.7 \mu\text{m} \times 30.7 \mu\text{m}$ were obtained.

PXCT measurement. PXCT experiments were performed at the cSAXS beamline (X12SA) of the Swiss Light Source, Paul Scherrer Institut, using X-rays of photon energy 6.2 keV. FIB fabricated cubic-shaped coating samples were measured. X-ray diffraction patterns in the transmission geometry were recorded by a PILATUS²⁸ photon-counting detector (pixel size $172 \mu\text{m} \times 172 \mu\text{m}$), placed 7.2 meters downstream of the samples. During the measurements, the samples were rotated 180° with 0.5° intervals, obtaining projections of the samples at 360 orientations. At each orientation angle, the samples were scanned along circular shells with a 1.4 μm radial step²⁹ in a plane perpendicular to the X-ray beam to cover a field of view extending



beyond the sample edges. The projections were reconstructed by the difference map algorithm²², then post-processed, aligned, combined and reconstructed to form a 3D volume according to the procedure described in reference 14.

- Biegańska, B., Zubielewicz, M. & Smieszek, E. Influence of barrier pigments on the performance of protective organic coatings. *Prog. Org. Coat.* **16**, 219–229 (1988).
- Thomas, N. L. The barrier properties of paint coatings. *Prog. Org. Coat.* **19**, 101–121 (1991).
- Moggridge, G. D., Lape, N. K., Yang, C. & Cussler, E. L. Barrier films using flakes and reactive additives. *Prog. Org. Coat.* **46**, 231–240 (2003).
- Walter, G. W. A critical review of the protection of metals by paints. *Corros. Sci.* **26**, 27–38 (1986).
- Shreir, L. L., Jarman, R. A. & Burstein, G. T. (Eds.) *Corrosion* (3rd ed.): Chap. 14 (Butterworth-Heinemann Ltd., Oxford-London, 1994).
- Yang, C., Smyrl, W. H. & Cussler, E. L. Flake alignment in composite coatings. *J. Membrane Sci.* **231**, 1–12 (2004).
- Leidheiser, H., Jr., Wang, W. & Igetoft, L. The mechanism for the cathodic delamination of organic coatings from a metal surface. *Prog. Org. Coat.* **11**, 19–40 (1983).
- Müller, B. & Fischer, S. Epoxy ester resins as corrosion inhibitors for aluminium and zinc pigments. *Corros. Sci.* **48**, 2406–2416 (2006).
- Jaeggi, C., Mooser, R., Frauchiger, V. & Wyss, P. 3D characterization of open porous vacuum plasma sprayed titanium coatings by means of high resolution micro computer tomography. *Mater. Lett.* **63**, 2643–2645 (2009).
- Koller, D. M., Hanneschläger, G., Leitner, M. & Khinast, J. G. Non-destructive analysis of tablet coatings with optical coherence tomography. *Eur. J. Pharm. Sci.* **44**, 142–148 (2011).
- Lambourne, R. & Strivens, T. A. *Paint and Surface Coatings-Theory and Practice* (2nd ed.): 91–165 (Woodhead Publishing Ltd., Cambridge, England, 1999).
- Denk, W. & Horstmann, H. Serial block-face scanning electron microscopy to reconstruct three-dimensional tissue nanostructure. *PLoS Biol.* **2**, e329 (2004).
- Dierolf, M. *et al.* Ptychographic X-ray computed tomography at the nanoscale. *Nature* **467**, 436–439 (2010).
- Guizar-Sicairos, M. *et al.* Phase tomography from x-ray coherent diffractive imaging projections. *Opt. Express* **19**, 21345–21357 (2011).
- Levinthal, C. & Ware, R. Three dimensional reconstruction from serial sections. *Nature* **236**, 207–210 (1972).
- Arenkiel, B. R. & Ehlers, M. D. Molecular genetics and imaging technologies for circuit-based neuroanatomy. *Nature* **461**, 900–907 (2009).
- Rouquette, J. *et al.* Revealing the high-resolution three-dimensional network of chromatin and interchromatin space: A novel electron-microscopic approach to reconstructing nuclear architecture. *Chromosome Res.* **17**, 801–810 (2009).
- Müller-Reichert, T., Mancuso, J., Lich, B. & McDonald, K. Three-dimensional reconstruction methods for caenorhabditis elegans ultrastructure. *Methods Cell Biol.* **96**, 331–361 (2010).
- Briggman, K. L., Helmstaedter, M. & Denk, W. Wiring specificity in the direction-selectivity circuit of the retina. *Nature* **471**, 183–188 (2011).
- O'Brien, H. C. & McKinley, G. M. New microtome and sectioning method for electron microscopy. *Science* **98**, 455–456 (1943).
- Rodenburg, J. M. *et al.* Hard-X-Ray lensless imaging of extended objects. *Phys. Rev. Lett.* **98**, 034801 (2007).
- Thibault, P. *et al.* High-resolution scanning X-ray diffraction microscopy. *Science* **321**, 379–382 (2008).
- Glenn, W. V., Jr., Johnston, R. J., Morton, P. E. & Dwyer, S. J. Image generation and display techniques for CT scan data-Thin transverse and reconstructed coronal and sagittal planes. *Invest. Radiol.* **10**, 403–416 (1975).
- Kak, A. C. & Slaney, M. *Principles of Computerized Tomographic Imaging* (Society of Industrial and Applied Mathematics, Philadelphia, PA, 2001).
- Diaz, A. *et al.* Quantitative x-ray phase nanotomography. *Phys. Rev. B* **85**, 020104(R) (2012).
- Alam, P., Byholm, T., Kniivilä, J., Sinervo, L. & Toivakka, M. Calculating the permeability of model paper coating structures comprising incongruent particle shapes and sizes. *Micropor. Mesopor. Mat.* **117**, 685–688 (2009).
- Zaarei, D., Sarabi, A. A., Sharif, F. & Kassiriha, S. M. Structure, properties and corrosion resistivity of polymeric nanocomposite coatings based on layered silicates. *J. Coat. Technol. Res.* **5**, 241–249 (2008).
- Henrich, B. *et al.* PILATUS: A single photon counting pixel detector for X-ray applications. *Nucl. Instrum. Meth. A* **607**, 247–249 (2009).
- Dierolf, M. *et al.* Ptychographic coherent diffractive imaging of weakly scattering specimens. *N. J. Phys.* **12**, 035017 (2010).

Acknowledgements

The work was supported by the Engineering and Physical Sciences Research Council (EPSRC, UK) through a Dorothy Hodgkin Postgraduate Award to B.C. Additional funding came from the European Research Council (ERC) Advanced Grant 227711 “nanosculpture”. The PXCT experiments were carried out at the cSAXS beamline at the Swiss Light Source, Paul Scherrer Institut, Villigen PSI, Switzerland. The SBFSEM measurements were performed on the Gatan 3View system at Gatan Inc. B.C. acknowledges travel support from the European Community’s Seventh Framework Programme (FP7/2007–2013) through grant no. 226716. We acknowledge Dr. Paul Jackson at AkzoNobel (UK) for discussions.

Author contributions

I.R., B.C., F.V. and A.B. conceived the project. J.M. and A. M. carried out the SBFSEM measurements. B.C. analysed the SBFSEM result. B.C., S.H., F.V. and A.B. prepared samples for PXCT experiments. B.C., M.G., L.S., A.D. and N.B. carried out the PXCT experiments. B.C. and M.G. analysed the PXCT results. G.X., J.N. and B.C. carried out the COMSOL simulation. All authors contributed to interpreting the results and writing the manuscript.

Additional information

Supplementary information accompanies this paper at <http://www.nature.com/scientificreports>

Competing financial interests: The authors declare no competing financial interests.

License: This work is licensed under a Creative Commons Attribution-NonCommercial-NoDerivs 3.0 Unported License. To view a copy of this license, visit <http://creativecommons.org/licenses/by-nc-nd/3.0/>

How to cite this article: Chen, B. *et al.* Three-Dimensional Structure Analysis and Percolation Properties of a Barrier Marine Coating. *Sci. Rep.* **3**, 1177; DOI:10.1038/srep01177 (2013).